Hindawi Publishing Corporation
ISRN Biomedical Engineering
Volume 2013, Article ID 919802, 9 pages
http://dx.doi.org/10.1155/2013/919802

Research Article

Diffusion in Replica Healthy and Emphysematous Alveolar Models Using Computational Fluid Dynamics

Edward M. Harding Jr., Emily J. Berg, and Risa J. Robinson

Department of Mechanical Engineering, Kate Gleason College of Engineering, Rochester Institute of Technology, 76 Lomb Memorial Drive, Building 9, Rochester, NY 14623, USA

Correspondence should be addressed to Risa J. Robinson; rjreme@rit.edu

Received 11 March 2013; Accepted 8 May 2013

Academic Editors: A. Qiao and C. Thielemann

Deposition of nanosized particles in the pulmonary region has the potential of crossing the blood-gas barrier. Experimental *in vivo* studies have used micron-sized particles, and therefore nanoparticle deposition in the pulmonary region is not well understood. Furthermore, little attention has been paid to the emphysematous lungs, which have characteristics quite different from the healthy lung. Healthy and emphysematous replica acinus models were created from healthy and diseased human lung casts using three-dimensional reconstruction. Particle concentration and deposition were determined by solving the convective-diffusion equation numerically for steady and unsteady cases. Results showed decreased deposition efficiencies for emphysema compared to healthy lungs, consistent with the literature and attributed to significant airway remodeling in the diseased lung. Particle diffusion was found to be six times slower in emphysema compared to healthy model. The unsteady state simulation predicted deposition efficiencies of 96% in the healthy model for the 1 nm and 3 nm particles and 94% and 93% in the emphysema model for the 1 nm and 3 nm particles, respectively. Steady state was achieved in less than one second for both models. Comparisons between steady and unsteady predictions indicate that a steady-state simulation is reasonable for predicting particle transport under similar conditions.

1. Introduction

Emphysema is a chronic obstructive pulmonary disease characterized by irreversible damage to alveolar sacs in the pulmonary region of the lung [1, 2]. Specifically, the septa separating the individual acini are destroyed so that the tiny acini merge together to create one large air sac. The effect of emphysema-related lung remodeling on airflow and particle deposition is currently unknown. Understanding how deposition changes in the pulmonary region due to emphysema will help to improve differential risk assessment for those suffering from the disease as well as increase the accuracy of delivering inhaled medication used to treat disease.

Studies that model pulmonary airflow and deposition, both experimentally and numerically, are summarized in Table 1, including model characteristics and deposition mechanisms addressed in each study. Deposition in the pulmonary region is governed primarily by diffusion and sedimentation. Whole lung models, such as MPPD, Trumpet, and NCRP [3–5], use analytical deposition equations derived by Ingham [6–8] for straight tube geometries, whereas alveolar models have been published that account for the presence of individual acinar geometry. Some of the first studies made use of axisymmetry to create simplistic models of individual acini, whereas more recent models have begun to move closer to what many may consider actual geometries. Kumar et al. [9] and Sznitman et al. [10] presented a branching bronchiole numerical model with multihedron acini, and Berg et al. [11] presented a replica alveolar sac experimental model made from scans of human lung casts. No study has presented numerical results for diffusional deposition in replica alveolar geometries.

Studies that measured pulmonary deposition *in vivo* are summarized in Table 2. To some extent, the *in vivo* studies validated whole lung model predictions (Figure 1); however there is limited data for submicron-sized particles. Even fewer studies have looked at how the differences in healthy and

Table 1: Summary of whole lung models and alveolar models found in the literature.

Category	Study	Alveolar model geometry	Expanding	Emphysema	Particle deposition	
					Sedimentation	Diffusion
Whole lung models	NCRP [3]	Straight tube			X	X
	Yu and Diu (Trumpet) [5]	Straight tube			X	X
	Anjilvel and Asgharian (MPPD) [4]	Straight tube			X	X
	Sturm and Hofmann [12]	Round		X	X	X
Alveolar models						
Numerical	Tsuda et al. [13]	Round	X			
	Darquenne [14]	Round				X
	Haber et al. [15]	Round	X			X
	Sznitman et al. [16]	Round	X			
	Kumar et al. [9]	Octahedron	X			
	Sznitman et al. [10]	14-Hedron	X		X	
	Harding and Robinson [17]	Round	X			
Experimental	Karl et al. [18]	Square				
	Oakes et al. [19]	Round	X	X		
	Berg et al. [11]	Replica	X			
	Berg and Robinson [20]	Replica	X	X		

Table 2: Experimental studies involving pulmonary deposition (NR: not reported). Data is combined and plotted in Figure 1.

Study	Breathing frequency	n	Particle size (μm)
Lippmann and Albert [21]	14 breaths/minute	34	1.3–7.9
Pavia et al. [22]	NR	50	5 ± 0.7
Chan and Lippmann [23]	14 breaths/minute	26	0.2–7
Stahlhofen et al. [24]	NR	3	0.5–5
Stahlhofen et al. [25]	7.5 breaths/minute	9	5 and 7
Emmett et al. [26]	10 breaths/minute	12	3.5–10
Kim and Jaques [27]	15 breaths/minute	22	0.04–0.1

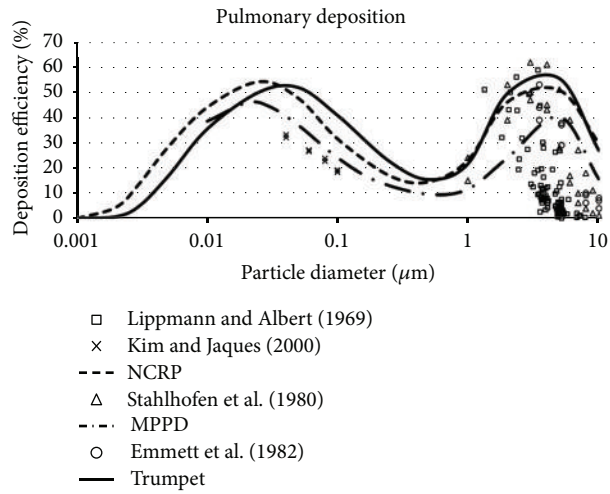

Figure 1: Whole lung model pulmonary deposition predictions compared to pulmonary deposition measurement studies listed in Table 2. Kim and Jaques [27] data show the average for 22 subjects.

emphysematous lung geometries affect particle transport and deposition. Sturm and Hofmann [12] presented a numerical model for particle deposition by the combined mechanisms of sedimentation and diffusion using various models of emphysema, for 0.001 to 10 μm particles in generations from the 12th to terminal. Particle deposition was shown to be higher in the healthy model compared to models representing various types of emphysema. Oakes et al. [19] and later Berg and Robinson [20] measured flow fields in idealized and replica models, respectively, by particle image velocimetry and found flow characteristics that would imply decreased deposition in emphysema compared to healthy. Kohlhäufl et al. [28] measured, on average, a greater bolus dispersion in 29 emphysema subjects compared to 79 healthy patients [29], which they attributed to airway blockage, unequal spread of the disease, and uneven ventilation.

In summary, limited data are available to describe the nature of diffusional particle deposition in the alveolar region, relying only on the whole lung models. Limited experimental data is available to validate whole lung models for particles in the submicron region. In our previous work, we showed that in the alveolar region, diffusive motion likely dominates for submicron particles [11, 17]. However, alveolar models to date have focused on sedimentation and to our knowledge, no study on diffusional deposition has been presented. The limited studies to date indicate that deposition is decreased in emphysema; however, more work is needed to fully characterize and understand the effects of diseased lung remodeling. In the present study, pure diffusional transport is simulated numerically in alveolar replica models of healthy and emphysemic geometries.

2. Methods

2.1. Model Creation. The healthy and emphysemic geometric models used in this study were previously used to measure

Table 3: Steady-state (SS) times, deposition efficiencies, and percent error associated with the steady-state approximation for various residence times.

Particle size	Healthy (H)		Emphysema (E)	
	1 nm	3 nm	1 nm	3 nm
Deposition from unsteady simulation	96%	96%	94%	93%
SS time (seconds)	0.08	0.26	0.17	0.49
Percent that steady-state simulation overestimates unsteady simulation results				
Residence time				
SS time	0.50%	1.46%	1.06%	4.12%
1 s	0.04%	0.38%	0.18%	1.98%
5 s	0.01%	0.08%	0.04%	0.39%

flow fields by particle image velocimetry [20]. Healthy and emphysematous human cadaver lungs were cast using the procedure of Phalen et al. [30]. Microscope pictures were taken of each of the casted pieces to determine which sections would be used for final reconstruction. Healthy humans typically have alveolar mouth diameters of approximately 230 to 336 μm [31, 32] and represent defined bulb structures. Our healthy human cast was within this range, measuring between 243 and 378 microns. The literature cites emphysematous diameters ranging from 430 to 830 μm [31] while our model's average effective airway diameter measures 1556 microns, indicating that our model was obtained from a severely diseased lung. Chosen sections were cut from the larger cast and scanned using microscale computed tomography (microCT) (Micro Photonics, Allentown, PA, USA). The healthy lung cast, measuring roughly 6 mm in size, was scanned at 3.58 μm/pixel and created 1,241 two-dimensional (2D) images, each containing a 2000 × 2000 pixel image with a file size of about 4000 KB. The emphysematous lung cast, measuring about 12 mm in size, was scanned at 3.35 μm/pixel, which produced 3,550 2D images, each a 4000 × 4000 pixel image approximately 15,300 KB in size. A representative example of a 2D image from the microCT scan is shown in Figure 2.

The lung models were reconstructed from the 2D images using 3D Doctor (Able Software, Lexington, MA, USA), applying a thresholding segmentation technique. Thresholding values between the limits of 45 and 255 provided the most optimal results, as it included the largest majority of the cast surface without including too much of the surrounding static. After examining the preliminary reconstructions (Figures 3(a) and 3(b)), smaller sections were chosen (Figures 3(c) and 3(d)) which reduced the total number of 2D images to 492 in the healthy model and 919 for the emphysematous. Only these regions were further processed and cleaned, while the other portions present in the image were deleted. Figures 3(e) and 3(f) show the original casts for comparison of the final reduced sections. This final reduction in the model size was done to reduce the number of 2D images that would require detailed image cleanup, to reduce the total number of meshed elements below the maximum supported by available RAM, and to reduce the overall computational time for simulation.

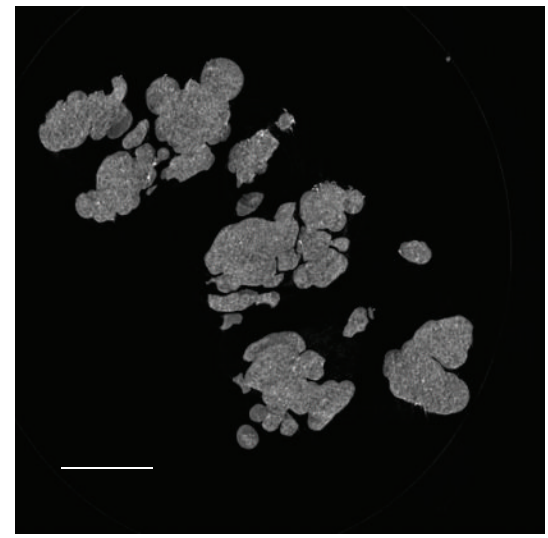

(a)

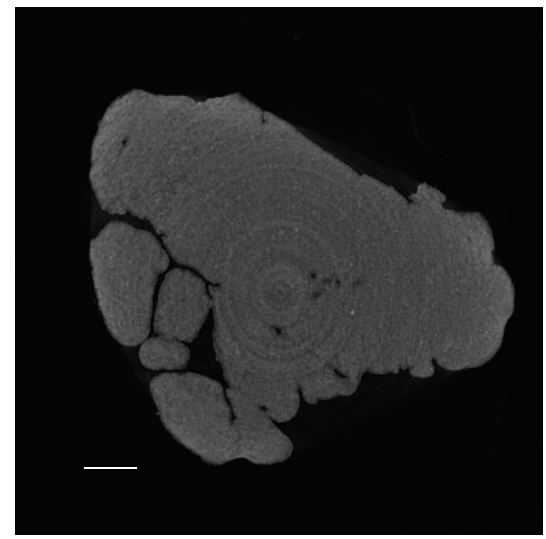

(b)

Figure 2: Examples of microCT image slices shown in ImageJ from (a) the healthy lung cast and the (b) the emphysema lung cast. The white line in the images represents 1 mm.

The final healthy model consisted of 368,238 nodes and 736,416 faces, while the emphysema final model had 1,589,498 nodes and 3,174,083 faces.

After reconstructions were done in 3D Doctor, object files, or OBJ files, were created for each of the models and exported to allow an easy transition into VP Sculpt (Colorado State University, Fort Collins, CO, USA) for surface cleanup to prepare the model for meshing. Each model was smoothed roughly fifty times to eliminate any outlying features, while maintaining the original number of faces and nodes that make up the model's surface. The models were then decimated, which is a process that combines similar faces to create larger faces, thereby reducing the model size without losing detail to the surface. It was necessary to decimate the models four times before the size was reduced enough for importing into SolidWorks (Solid Works Corp., Waltham, MA, USA) for model scaling. The healthy human model was reduced to 27,012 nodes and 54,032 faces after decimating, while the emphysemic human model was reduced to 23,497 nodes and 46,982 faces.

Finally, improper, null, and appended facets and unconnected vertices that may have resulted from either the reconstruction or smoothing and decimation processes were removed, and outer boundaries and holes were filled in order to produce a complete volume. The final step was to scale the models to accurately depict the original *in vivo* dimensions. SEM (scanning electron micrographs) and high-powered microscope images were analyzed using ImageJ to determine millimeter (mm) to pixel conversion factors. A scaling factor of 0.00361 pixels/mm was used for the healthy model, and a factor of 0.00306 pixels/mm was used for the emphysemic model.

The final healthy human model extends 2.11 mm in the x-direction, 1.34 mm in the y-direction, and 1.74 mm in the z-direction with an inlet duct diameter of 0.41 mm. The total volume of the model was 1.16 mm^3 with a total surface area of 10.46 mm^2. The emphysema human model had a total volume of 12.49 mm^3 and surface area of 33.56 mm^2 and is 10.8 times larger than the healthy model by volume. The global size of the model measures 3.74 mm, 3.18 mm, and 3.49 mm in the x, y, and z directions, respectively, with an inlet duct diameter of 0.81 mm. These dimensions are well within published values [28, 31–34].

2.2. Mesh Generation. Meshing was done in Harpoon (Sharc Ltd., Manchester, UK), an automatic hex dominant volume meshing software. The models were exporting from VP Sculpt as STL files and imported into Harpoon as one complete surface, which was then broken into two faces, the inlet surface and acinus walls. The healthy model was meshed using a max volume size of 0.04 and a surface cell size of 0.010, which created 774,380 elements and 627,214 nodes (Figure 4(a)). The surface cell size was approximately 0.6% of the healthy model's x, y, and z dimensions, similar to the initial boundary layer height of 0.5% of the radial and axial dimensions of the tube used in the Chen validation [35]. The max volume size is 2.4% on average of the model's dimensions, which also compares well with the internal mesh of 2.5% of the dimensions used in Chen's work. The emphysemic model was meshed using a base level of 0.025, a surface cell size of 0.01250, or 0.4% of the model's size, and max volume size of 0.02500, or 0.7% of the overall size, which created 947,199 elements and 842,689 nodes (Figure 4(b)). An example of the hex-meshing scheme is shown in a blown-up portion of the healthy model (Figure 4(c)).

2.3. Theory of Brownian Diffusion and Convective-Diffusion Equation. Fick's law of diffusion was applied to solve for particle transport in the healthy and emphysemic models. Particle diffusion is the mass transfer of particles from a region of higher concentration to a region of lower concentration, as a result of Brownian motion or random particle motion due to the random relentless bombardment of gas molecules [36]. Fick's first law of diffusion is given by

$$J = -D\nabla C, \tag{1}$$

where J is the flux vector (particles/m^2 s), D is the diffusion coefficient (m^2/s), and $C(x, y, z, t)$ is the particle concentration (particles/m^3). If Fick's first law is applied to a finite volume element, along with the conservation of mass theorem, the particle concentration can be found by solving the convection-diffusion equation for zero mass generation [37] by

$$\frac{\partial C}{\partial t} = \nabla \cdot [D\nabla C], \tag{2}$$

where t is the time. Total particle diffusion through any given surface area, J'_{area} (particles/s), can be found by integrating $C(x, y, z, t)$ over the surface area, A_{area}, using

$$J'_{\text{area}} = \int_{\text{area}} -D \left.\frac{\partial C}{\partial \hat{x}}\right|_{\text{area}} dA_{\text{area}}, \tag{3}$$

where x is the direction normal to the surface area. Equation (3) can be integrated over the inlet surface area to determine the rate of particle diffusion into the mode, J'_{inlet}, and integrated over the wall surface area, J'_{wall}, to determine diffusional deposition on the model wall. Total diffusion can be found by summing (3) over time, t, so that deposition efficiency can be determined from

$$\text{deposition efficiency} = \frac{\int_t \int_{\text{wall}} -D\,(\partial C/\partial \hat{x})|_{\text{wall}} dA_{\text{wall}} dt}{\int_t \int_{\text{inlet}} -D\,(\partial C/\partial \hat{x})|_{\text{inlet}} dA_{\text{inlet}} dt} \times 100\%. \tag{4}$$

2.4. Numerical Techniques. The convective-diffusion equation was solved to obtain concentration as a function of position and time using the Fine Particle Model (FPM), which is a user defined subroutine (UDF) for the Computational Fluid Dynamics (CFD) software package, FLUENT (ANSYS, Inc., Canonsburg, PA, USA) [38]. The FPM solves an equation known as the Moment Dynamics Equation,

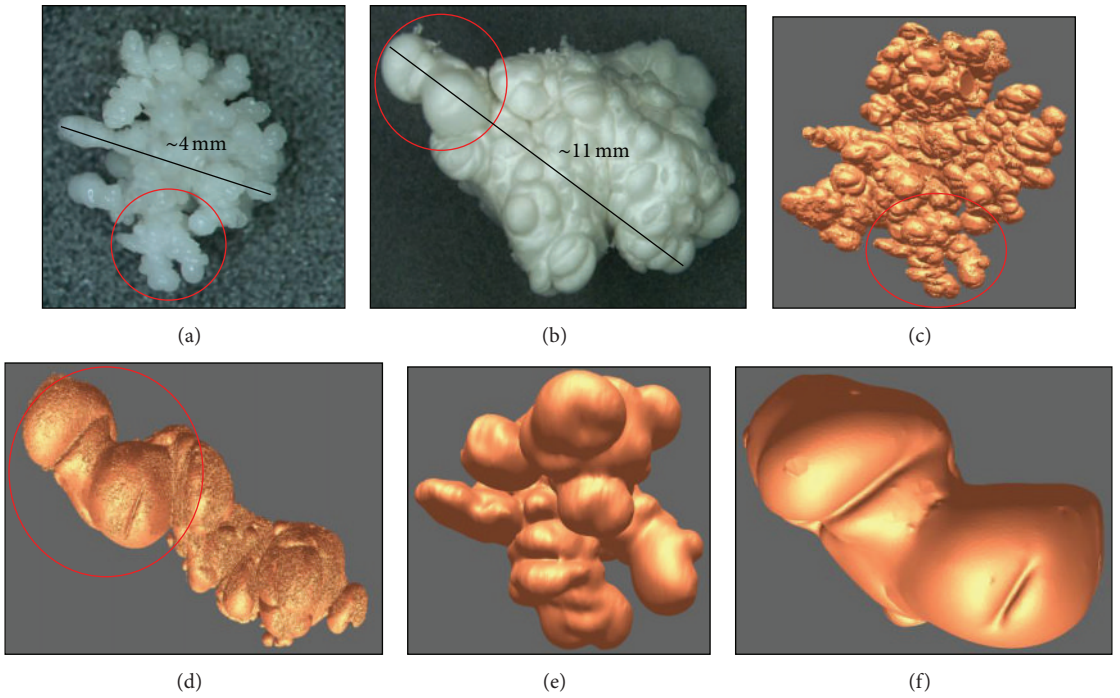

Figure 3: Original (a) healthy and (b) emphysemic casts. The red circles represent the sections chosen for final models, while the black lines demonstrate model scales. Whole model reconstructions of (c) healthy and (d) emphysemic models and the final chosen sections for the (e) healthy and (f) emphysemic models.

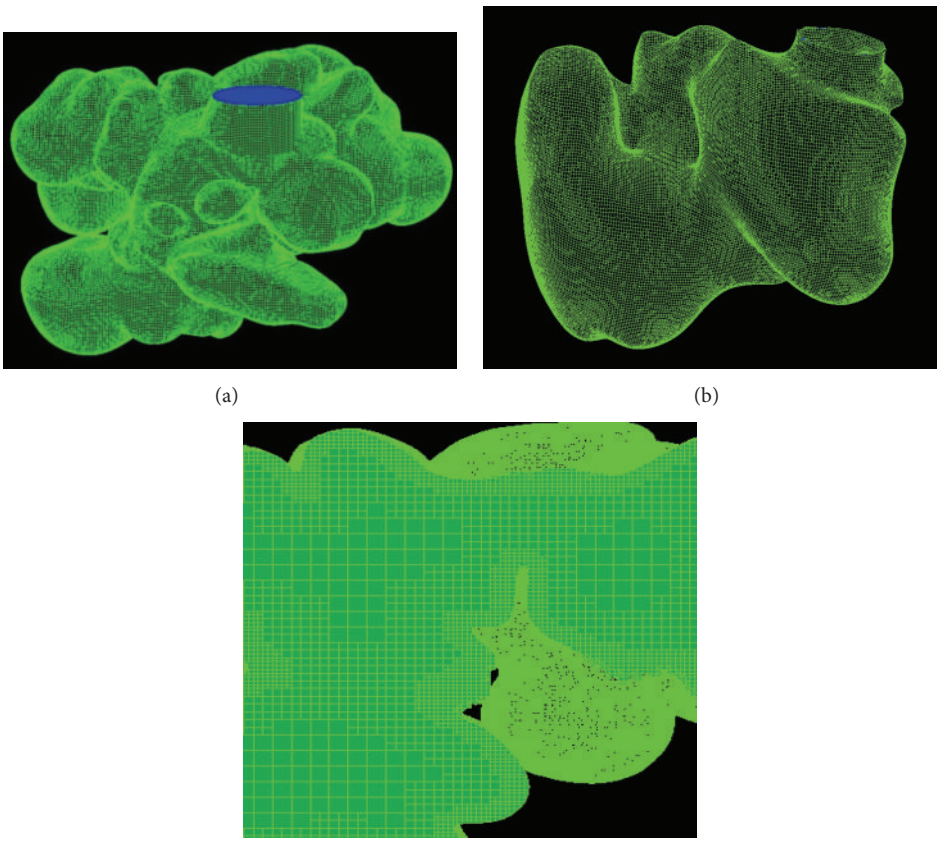

Figure 4: Meshed (a) healthy and (b) emphysemic models and (c) an example of the the hex meshing scheme.

which is simplified to (2) for monodisperse aerosols dominated by diffusion. The particle flux at the inlet, J'_{inlet}, and the wall, J'_{wall}, was extracted from the CFD/FPM analysis after each simulation time step. The deposition efficiencies were determined manually by applying (4) to the exported particle flux data.

A constant inlet concentration of 1e15 particles/m^3 was set at each of the model inlets, while the wall boundary conditions were set to a concentration of 0 particles/m^3. Particle sizes of 1 nm and 3 nm diameter were analyzed for a period of 5 seconds.

3. Results

3.1. Concentration Contours in Healthy and Emphysema Models. Unsteady concentration contours in the healthy and emphysemic models were taken at an x-y plane located in the center of the inlet duct for 1 and 3 nm particles. Figure 5 shows the concentration contours for the 3 nm particles in the healthy and emphysematous models at three points in time during the simulation period. Similar contours were obtained for the 1 nm particle (not shown). For both particle sizes, a larger time was needed to penetrate the emphysemic model compared to the healthy mode, and to a lesser extent, larger times were needed for the emphysemic model to reach steady-state contours compared to the healthy model.

For both the 1 nm and 3 nm particles, the emphysemic model took 6 times longer to reach similar concentration profiles compared to the healthy model, and steady state was reached in half the time for the healthy compared to the emphysemic model. The associated times for the 3 nm results are provided in Figure 5. For the 1 nm particles (not shown), the emphysemic model took 0.006 sec to reach the same penetration depth shown in Figure 5 (middle row), while the healthy model took only 0.001 sec. Furthermore, for the 1 nm particle, steady state was reached in 0.08 sec for the healthy model compared to 0.17 sec for the emphysemic model.

As expected, the steady-state concentration contours were the same for both the 1 nm and 3 nm particles since at steady state, the diffusion coefficient no longer contributes to the solution of the concentration (2). Because steady state is reached relatively quickly, it is reasonable to consider the steady-state solution as a first approximation for deposition calculations that rely on these particle concentration contours.

Steady-state particle contours are shown in Figure 6 for both the healthy and emphysemic models. Each model was sectioned into six planes. The healthy model planes are equally spaced by 0.248 mm, while the emphysemic model planes are equally spaced by 0.499 mm. Since these are steady-state concentrations, they are independent of particle size. It is evident from these isometric images that the emphysemic model has a much lower concentration of inhaled particles distributed throughout the airway volume as compared to the healthy model. These differences in concentration gradient, particularly near the airway wall, will result in smaller particle deposition for emphysemic lungs compared to healthy lungs.

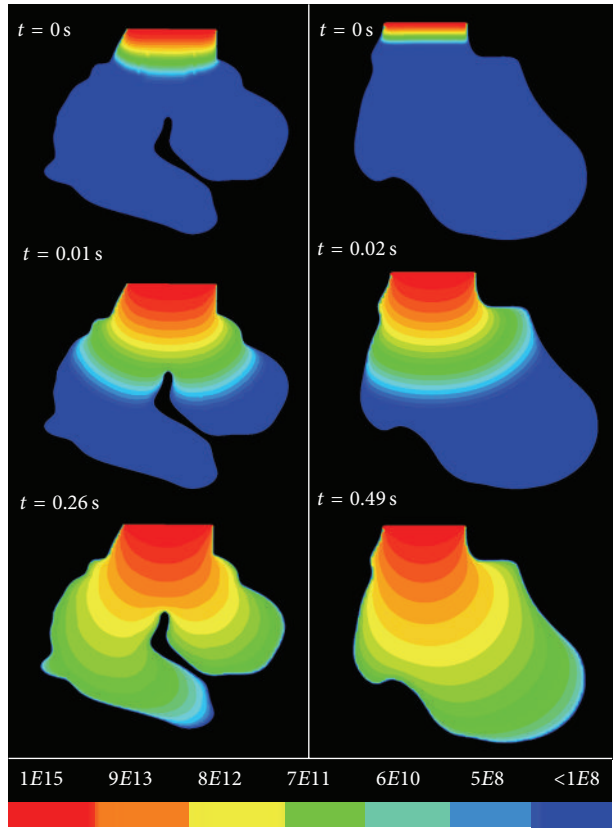

Figure 5: Unsteady concentration contours (particles/mm^3) for 3 nm particles, for the times shown. Bottom row contours are at steady state for each model. Left and right panels are for the healthy and emphysemic models, respectively. The plane shown is located at the center of each model's inlet.

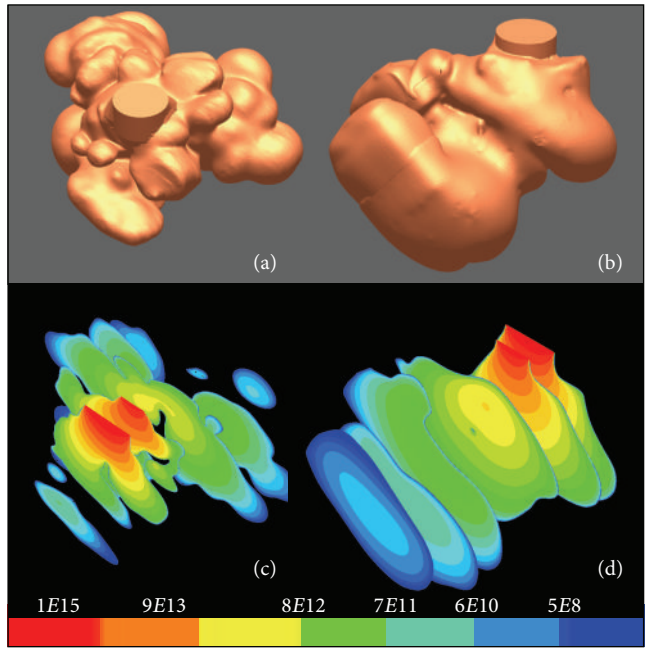

Figure 6: (a) Healthy and (b) emphysemic model renderings in VP Sculpt. Steady-state concentration contours (particles/mm^3) for the (c) healthy and (d) emphysemic models.

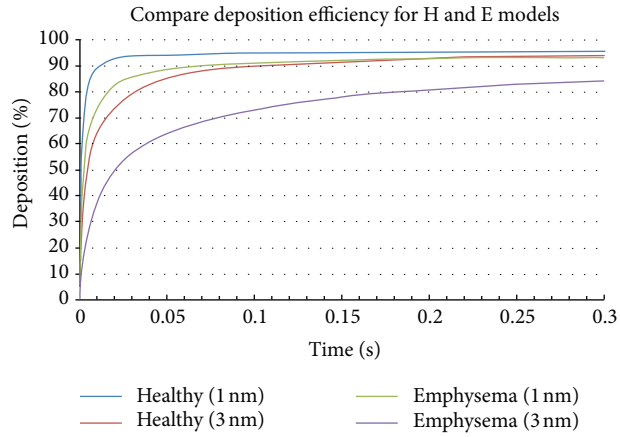

Figure 7: Plot showing the percent deposition of particles entering the healthy and emphysemic models for particle sizes of 1 nm and 3 nm over a 2-second period.

3.2. Diffusional Deposition in Healthy and Emphysemic Models. Total particle deposition in the healthy and emphysemic models was obtained by summing the wall flux output over various time periods using (3). The deposition efficiency was calculated using (4). Figure 7 shows the percent deposition for 1 nm and 3 nm particles in the healthy and emphysemic models over a 2-second period. The deposition rate is larger for the healthy model compared to the emphysemic model for both particle sizes. Figure 7 also demonstrates that each model simulation quickly approached steady state, more quickly for the healthy compared to the emphysemic model and for the 1 nm compared to 3 nm particle size (Table 3).

Assuming steady-state deposition over the entire breathing period provides the opportunity to simplify the numerical simulation. The error associated with the steady-state assumption is provided in Table 3 for a range of particle residence times, assuming that steady state occurs when the slope of the deposition efficiency curve becomes less than 0.1% per second (Figure 7). The 1 nm healthy simulation reached steady state at 0.08 sec. The worst case shown is for a 3 nm particle in the emphysemic model, where the steady simulation yields a 4.12% overestimation compared to the unsteady simulation for 0.49 second residence time. The error reduces for larger, more realistic residence times. Therefore, it appears that the steady-state assumption is reasonable.

4. Discussion

4.1. Effect of Emphysema on Particle Deposition. The simulated deposition efficiencies for the emphysema model are less than the healthy model. Decreased deposition in emphysema can be attributed to alveolar remodeling due to the destruction of the septa walls. The large, nonbranching volume of the diseased sac results in larger diffusion distances and smaller particle concentration gradients in the emphysemic compared to the healthy lung, as shown in the simulation results. It takes longer for the particles to reach an alveolar surface in emphysema and longer to develop a steady-state particle concentration gradient. Once the particle gradient reaches steady state, the magnitude of the gradient, which is the driving force behind diffusive particle transport and deposition, is much smaller in emphysema compared to the healthy lung.

4.2. Comparison of Numerical and Experimental Studies. Simulations presented in this study are consistent with the numerical predictions of Sturm and Hoffmann [12], in which they reported a 7% decrease in pulmonary region deposition of emphysema compared to healthy and are consistent with decreased deposition in animal models with emphysema [39–43].

Experimental studies of particle deposition in the submicron range are not available for comparison of simulation results of the present study. The smallest experimental data point is a mean deposition efficiency of 33% for 0.04 microns, reported by Kim and Jaques [27] for healthy humans (Figure 1). The experimental trend in the range from 0.1 to 0.4 microns is reported to be an increase in deposition efficiency for decreasing particle size.

5. Conclusions

Two *in vivo* replica alveolar models, healthy and emphysematous, were created using lung casting and three-dimensional reconstruction techniques. The resulting geometries of the healthy and emphysemic models were consistent with the literature in terms of general features, sizes, and shapes of the alveoli. The healthy and emphysemic models were simulated to determine deposition of 1 nm and 3 nm particles by pure diffusion, for the same inhaled particle concentration. The study predicts very high and localized deposition in the alveolar sacs, with a decreased efficiency for emphysemic compared to the healthy lung, which can be attributed to geometric remodeling as a result of alveolar wall destruction. Results agree qualitatively with *in vivo* experimental published data reporting decreased deposition in emphysema compared to healthy lungs. Additional studies are needed, both experimental and numerical, to better understand nanoparticle deposition in the pulmonary region of the lung.

Conflict of Interests

The authors of this paper do not have a direct financial relation with the commercial identities mentioned in the paper that might lead to a conflict of interests.

Acknowledgments

This work was supported by the American Cancer Society (RSG-05-021-01-CNE). The authors would like to thank Dr. Richard Doolittle (Vice Dean of RIT's College of Health Sciences and Technology) for his assistance in obtaining samples of healthy and emphysemic human lungs. This work is dedicated to the memory of Ted (Teddy) Harding Jr. (Mechanical Engineering Graduate, RIT).

References

[1] P. F. Adams, P. M. Barnes, and J. L. Vickerie, "Summary Health Statistics for the U.S. Population: National Health Interview Survey, 2007," *Vital and Health Statistics*, vol. 10, no. 238, pp. 1–104, 2008.

[2] A. S. Buist, M. A. McBurnie, W. M. Vollmer et al., "International variation in the prevalence of COPD (The BOLD Study): a population-based prevalence study," *The Lancet*, vol. 370, no. 9589, pp. 741–750, 2007.

[3] Ncrp, "Deposition, retention and dosimetry of inhaled radioactive substances," Ncrp Report 125, Bethesda, MD, USA, 1997.

[4] S. Anjilvel and B. Asgharian, "A multiple-path model of particle deposition in the rat lung," *Fundamental and Applied Toxicology*, vol. 28, no. 1, pp. 41–50, 1995.

[5] C. P. Yu and C. K. Diu, "Total and regional deposition of inhaled aerosols in humans," *Journal of Aerosol Science*, vol. 14, no. 5, pp. 599–609, 1983.

[6] D. B. Ingham, "Diffusion of aerosols from a stream flowing through a cylindrical tube," *Journal of Aerosol Science*, vol. 6, no. 2, pp. 125–132, 1975.

[7] D. B. Ingham, "Diffusion of aerosols from a stream flowing through a short cylindrical pipe," *Journal of Aerosol Science*, vol. 15, no. 5, pp. 637–641, 1984.

[8] D. B. Ingham, "Diffusion of aerosols in the entrance region of a smooth cylindrical pipe," *Journal of Aerosol Science*, vol. 22, no. 3, pp. 253–257, 1991.

[9] H. Kumar, M. H. Tawhai, E. A. Hoffman, and C. Lin, "The effects of geometry on airflow in the acinar region of the human lung," *Journal of Biomechanics*, vol. 42, no. 11, pp. 1635–1642, 2009.

[10] J. Sznitman, T. Heimsch, J. H. Wildhaber, A. Tsuda, and T. Rösgen, "Respiratory flow phenomena and gravitational deposition in a three-dimensional space-filling model of the pulmonary acinar tree," *Journal of Biomechanical Engineering*, vol. 131, no. 3, pp. 031010-1–031010-16, 2009.

[11] E. J. Berg, J. L. Weisman, M. J. Oldham, and R. J. Robinson, "Flow field analysis in a compliant acinus replica model using particle image velocimetry (PIV)," *Journal of Biomechanics*, vol. 43, no. 6, pp. 1039–1047, 2010.

[12] R. Sturm and W. Hofmann, "Stochastic simulation of alveolar particle deposition in lungs affected by different types of emphysema," *Journal of Aerosol Medicine*, vol. 17, no. 4, pp. 357–372, 2004.

[13] A. Tsuda, F. S. Henry, and J. P. Butler, "Chaotic mixing of alveolated duct flow in rhythmically expanding pulmonary acinus," *Journal of Applied Physiology*, vol. 79, no. 3, pp. 1055–1063, 1995.

[14] C. Darquenne, "A realistic two-dimensional model of aerosol transport and deposition in the alveolar zone of the human lung," *Journal of Aerosol Science*, vol. 32, no. 10, pp. 1161–1174, 2001.

[15] S. Haber, D. Yitzhak, and A. Tsuda, "Gravitational deposition in a rhythmically expanding and contracting alveolus," *Journal of Applied Physiology*, vol. 95, no. 2, pp. 657–671, 2003.

[16] J. Sznitman, F. Heimsch, T. Heimsch, D. Rusch, and T. Rösgen, "Three-dimensional convective alveolar flow induced by rhythmic breathing motion of the pulmonary acinus," *Journal of Biomechanical Engineering*, vol. 129, no. 5, pp. 658–665, 2007.

[17] E. M. Harding Jr. and R. J. Robinson, "Flow in a terminal alveolar sac model with expanding walls using computational fluid dynamics," *Inhalation Toxicology*, vol. 22, no. 8, pp. 669–678, 2010.

[18] A. Karl, F. S. Henry, and A. Tsuda, "Low Reynolds number viscous flow in an alveolated duct," *Journal of Biomechanical Engineering*, vol. 126, no. 4, pp. 420–429, 2004.

[19] J. M. Oakes, S. Day, S. J. Weinstein, and R. J. Robinson, "Flow field analysis in expanding healthy and emphysematous alveolar models using particle image velocimetry," *Journal of Biomechanical Engineering*, vol. 132, no. 2, 2010.

[20] E. J. Berg and R. J. Robinson, "Stereoscopic particle image velocimetry analysis of healthy and emphysemic alveolar sac models," *Journal of Biomechanical Engineering*, vol. 133, no. 6, Article ID 061004, 2011.

[21] M. Lippmann and R. E. Albert, "The effect of particle size on the regional deposition of inhaled aerosols in the human respiratory tract," *American Industrial Hygiene Association journal*, vol. 30, no. 3, pp. 257–275, 1969.

[22] D. Pavia, M. L. Thomson, S. W. Clarke, and H. S. Shannon, "Effect of lung function and mode of inhalation on penetration of aerosol into the human lung," *Thorax*, vol. 32, no. 2, pp. 194–197, 1977.

[23] T. L. Chan and M. Lippmann, "Experimental measurements and empirical modelling of the regional deposition of inhaled particles in humans," *American Industrial Hygiene Association Journal*, vol. 41, no. 6, pp. 399–409, 1980.

[24] W. Stahlhofen, J. Gebhart, and J. Heyder, "Experimental determination of the regional deposition of aerosol particles in the human respiratory tract," *American Industrial Hygiene Association Journal*, vol. 41, no. 6, pp. 385–398, 1980.

[25] W. Stahlhofen, J. Gebhart, and J. Heyder, "Biological variability of regional deposition of aerosol particles in the human respiratory tract," *American Industrial Hygiene Association Journal*, vol. 42, no. 5, pp. 348–352, 1981.

[26] P. C. Emmett, R. J. Aitken, and W. J. Hannan, "Measurements of the total and regional deposition of inhaled particles in the human respiratory tract," *Journal of Aerosol Science*, vol. 13, no. 6, pp. 549–560, 1982.

[27] C. S. Kim and P. A. Jaques, "Respiratory dose of inhaled ultrafine particles in healthy adults," *Philosophical Transactions of the Royal Society A*, vol. 358, no. 1775, pp. 2693–2705, 2000.

[28] M. Kohlhäufl, P. Brand, T. Meyer et al., "Detection of impaired intrapulmonary convective mixing by aerosol bolus dispersion in patients with emphysema," *European Journal of Medical Research*, vol. 2, no. 3, pp. 121–128, 1997.

[29] P. Brand, C. Rieger, H. Schulz, T. Beinert, and J. Heyder, "Aerosol bolus dispersion in healthy subjects," *European Respiratory Journal*, vol. 10, no. 2, pp. 460–467, 1997.

[30] R. F. Phalen, H. Yeh, O. G. Raabe, and D. J. Velasquez, "Casting the lungs in situ," *Anatomical Record*, vol. 177, no. 2, pp. 255–264, 1973.

[31] M. Kohlhäufl, P. Brand, G. Scheuch et al., "Aerosol morphometry and aerosol bolus dispersion in patients with CT-determined combined pulmonary emphysema and lung fibrosis," *Journal of Aerosol Medicine: Deposition, Clearance, and Effects in the Lung*, vol. 13, no. 2, pp. 117–124, 2000.

[32] B. Haefeli-Bleuer and E. R. Weibel, "Morphometry of the human pulmonary acinus," *Anatomical Record*, vol. 220, no. 4, pp. 401–414, 1988.

[33] M. Kohlhäufl, P. Brand, T. Selzer et al., "Diagnosis of emphysema in patients with chronic bronchitis: a new approach," *European Respiratory Journal*, vol. 12, no. 4, pp. 793–798, 1998.

[34] E. R. Weibel, "Lung Structure," *Medicina Thoracalis*, vol. 22, no. 5, p. 548, 1965.

[35] G. Chen, *Solution of Diffusion Equation in Axisymmetrical Coordinates*, Master of Science Ohio University, 1994.

[36] W. C. Hinds, *Aerosol Technology: Properties, Behavior, and Measurement of Airborne Particles*, John Wiley & Sons, 1999.

[37] B. Gebhart, *Heat Conduction and Mass Transfer*, McGraw-Hill, New York, NY, USA, 1993.

[38] T. Chimera, *Fine Particle Model (Fpm) for Fluent*, Evan Whitby, 2005.

[39] E. G. Damon, B. V. Mokler, and R. K. Jones, "Influence of elastase-induced emphysema and the inhalation of an irritant aerosol on deposition and retention of an inhaled insoluble aerosol in Fischer-344 rats," *Toxicology and Applied Pharmacology*, vol. 67, no. 3, pp. 322–330, 1983.

[40] D. L. Lundgren, E. G. Damon, J. H. Diel, and F. F. Hahn, "The deposition, distribution and retention of inhaled 239PuO2 in the lungs of rats with pulmonary emphysema," *Health Physics*, vol. 40, no. 2, pp. 231–235, 1981.

[41] J. C. Martin, H. Daniel, and L. Le Bouffant, "Experimental study of pulmonary emphysema in rats exposed to coal dust and papain: effects on the infrastructure and the cell dynamics," *American Industrial Hygiene Association Journal*, vol. 41, no. 1, pp. 12–19, 1980.

[42] F. F. Hahn and C. H. Hobbs, "The effect of enzyme-induced pulmonary emphysema in Syrian hamsters on the deposition and long-term retention of inhaled particles," *Archives of Environmental Health*, vol. 34, no. 4, pp. 203–211, 1979.

[43] J. L. Mauderly, D. E. Bice, Y. S. Cheng et al., "Influence of preexisting pulmonary emphysema on susceptibility of rats to inhaled diesel exhaust," *American Review of Respiratory Disease*, vol. 141, no. 5 I, pp. 1333–1341, 1990.